

## Experimental study of Fe-Ni-Ti-Cr system

Viktoria Hoppe\*, Anna Gibas\*, Weronika Grzegorzczuk\*,  
Marcin Małecki\*, Mariusz Hasiak\*\*

\* Wrocław University of Science and Technology, Faculty of Mechanical Engineering,  
5 Łukasiewicza St., 50-370 Wrocław, Poland

\*\* Wrocław University of Science and Technology, Department of Mechanics and Materials Science,  
25 Smoluchowskiego St., 50-370, Wrocław, Poland

**Abstract:** The research comprises a discussion about a formation of intermetallic phase with stoichiometric composition  $Fe_2Ti$ , called Laves phase, and influence of chromium on the whole structure containing this phase by means of comparison of the two alloys. A base  $Fe_{35}Ni_{35}Ti_{30}$  alloy was used as a reference and then compared with a Fe-Ni-Ti chromium doped -  $Fe_{30}Ni_{35}Ti_{30}Cr_5$  alloy. The study of microstructure performed with scanning electron microscope enabled to distinguish different phases. These regions are rich in mixture of Fe-Ni and Ti-Ni elements. The identified phases are  $Fe_2Ti$  and  $Ni_3Ti$  which was confirmed by X-ray diffraction and simultaneously it is consistent with energy dispersive spectroscopy results. Differential scanning calorimetry confirmed also multi-phase composition. As a result different hardness was measured for these phases using nanoindentation. The overall hardness was established using the Vickers method.

**Keywords:** mechanical properties, shape memory alloys, Fe-Ni-Ti alloy, Fe-Ni-Ti-Cr alloy

### 1. Introduction

Ni-based alloys are known for their extraordinary properties. Shape memory capability is gained by diffusionless phase transformation from austenite to martensite [1]. This transformation appears under two conditions - when there is stress applied to the material or temperature changes within the material. An addition of Fe to the traditional Ni-Ti alloy helps to decrease the transformation temperature [2].

Shape memory alloys are used as aerospace materials because of their high strength as well as impressive heat and corrosion resistance [3]. They find applications also in medical engineering [4].

Occurrence of intermetallic Laves phase in 300 K is characteristic for Fe-Ni-Ti alloys group (with approximate atomic composition 1:1:1) [5,6].  $Fe_2Ti$  phase has exceptional magnetic behavior. As its temperature increases it turns from antiferromagnet into paramagnet [7].

The goal of this research is to investigate changes in alloy structure, mechanical, physiochemical and magnetic properties of shape memory alloys with addition of chromium. The  $Fe_{30}Ni_{35}Ti_{30}Cr_5$  alloy properties were compared with one of the base alloy  $Fe_{35}Ni_{35}Ti_{30}$ .

### 2. Materials and methods

The  $Fe_{35}Ni_{35}Ti_{30}$  and  $Fe_{30}Ni_{35}Ti_{30}Cr_5$  (at. %) alloys were prepared in arc melter in argon protective atmosphere (99.999%). The purity of constituent elements exceeded 99%. The total mass of the specimens was about 10 g each. Both alloys were remelted five times to ensure homogeneity.

Phase analysis was performed with the help of an X-ray diffractometer Ultima IV (Rigaku) with  $CuK\alpha$  radiation, in the range of angles  $2\theta$  from  $20^\circ$  to  $90^\circ$  with a step of 0.05. The diffractograms were analyzed with usage of FindIt software utilizing the Inorganic Crystal

Structure Database Fiz Karlsruhe. Microstructure tests and chemical composition analysis were carried out by scanning electron microscope FESEM FEI Nova NanoSEM 230 with 1 nm resolution and the possibility of working in a low vacuum, equipped with an EDS spectrometer (EDAX Genesis). The investigations of temperature structure stability of the produced materials were executed by DSC/TGA (differential scanning calorimetry/ thermogravimetric analysis) measurements employing STA 449 F1 Jupiter instrument (Netzsch). The mechanical properties of the Fe-Ni-Ti and Fe-Ni-Ti-Cr alloys were measured with the help of nanoindenter (NHT, CSM Instruments NHT2) equipped with a Berkovich indenter. The experiment applied a load of 50 mN. The hardness of the material is a result of the maximum depth of the indenter and the Young's modulus resulting from the nature of the curve during unloading, were determined. Additionally, hardness measurements were made applying the Vickers method with MMT-X3 microhardness, in accordance with the EN ISO 6507-2: 1999 standard. The pressure exerted by the force of 9.81 N took place in 15 seconds. 100 hardness measurements were carried out for each sample.

### 3. Theoretical background

On the ternary equilibrium graph Fe-Ni-Ti, the point corresponding to the chemical composition of the alloy is marked (Fig 1). On the isothermal section corresponding to a temperature of 1000°C, occurrence of Fe<sub>2</sub>Ti and Ni<sub>3</sub>Ti phases is observed.

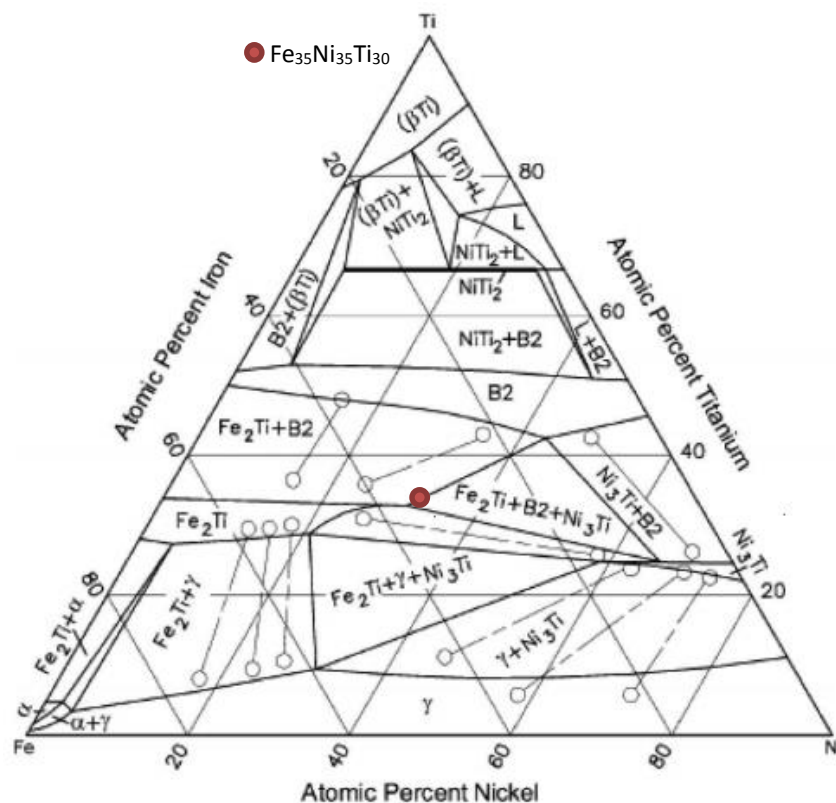


Fig. 1 Isothermal section of the Fe-Ni-Ti system at 1000°C [5].

Gamma prime phase –  $\gamma'$  (Ni<sub>3</sub>Ti) is a principal strengthening phase in many nickel- and nickel-iron- base superalloys. Crystal lattice varies slightly in size (0-0.5%) from that of austenite matrix. Its shape varies from spherical to cubic and size varies with exposure time and temperature [9].

Laves phase (Fe<sub>2</sub>Ti) is most common in iron-base superalloys. It usually appears as irregularly shaped globules, often elongated, or as platelets after extended high-temperature exposure [9].

## 4. Experimental study

The EDS analysis of the chemical composition was performed for different surface areas of the samples. In each case, the EDS analysis showed that the obtained alloy had a chemical composition corresponding to the nominal composition.

Tab. 1 Chemical composition of  $Fe_{35}Ni_{35}Ti_{30}$

at. %	Fe	Ni	Ti
Nominal composition	35.0	35.0	30.0
Measurement (EDS)	37.1	32.0	30.9

Tab. 2 Chemical composition of  $Fe_{30}Ni_{35}Ti_{30}Cr_5$

at. %	Fe	Ni	Ti	Cr
Nominal composition	30.0	35.0	30.0	5.0
Measurement (EDS)	34.5	33.8	27.0	4.7

Using the EDS detector, it is possible to perform qualitative and semi-quantitative chemical analyzes. The differences in the chemical composition on the surface of sample are visible on the maps of the distribution of elements.

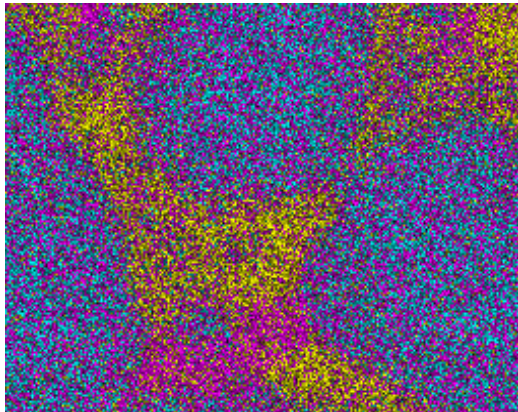


Fig. 2 Distribution of elements for the  $Fe_{35}Ni_{35}Ti_{30}$  (Fe – cyan, Ni – yellow, Ti – magenta) EDS mapping. 20000x. SEM - EDS. Acceleration voltage: 20kV

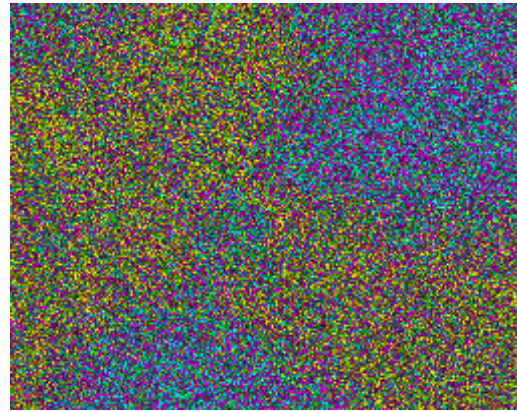


Fig. 3 Distribution of elements for the  $Fe_{30}Ni_{35}Ti_{30}Cr_5$  (Fe – cyan, Ni – yellow, Ti –magenta, Cr – green) EDS mapping. 20000x. SEM - EDS. Acceleration voltage: 20kV

There are Fe-Ti rich areas, which are characterized by globular particles and Ni-Ti rich areas as a matrix. (Fig 2). In the case of Fe-Ni-Ti-Cr alloy, an even distribution of chromium on the sample was observed. A similar distribution of Fe-Ti and Ni-Ti elements is visible on the surface of the second alloy (Fig 3).

SEM images confirm the existence of areas with different distribution of elements on the researched surface. There is a contrast associated with the different atomic mass of the elements that alloys are made. In the image they are visible lighter and darker fields and testify to dissolution (Fig 3). It can be assumed that chromium provokes the fragmentation of one of the structures and increases the interface (Fig. 4).

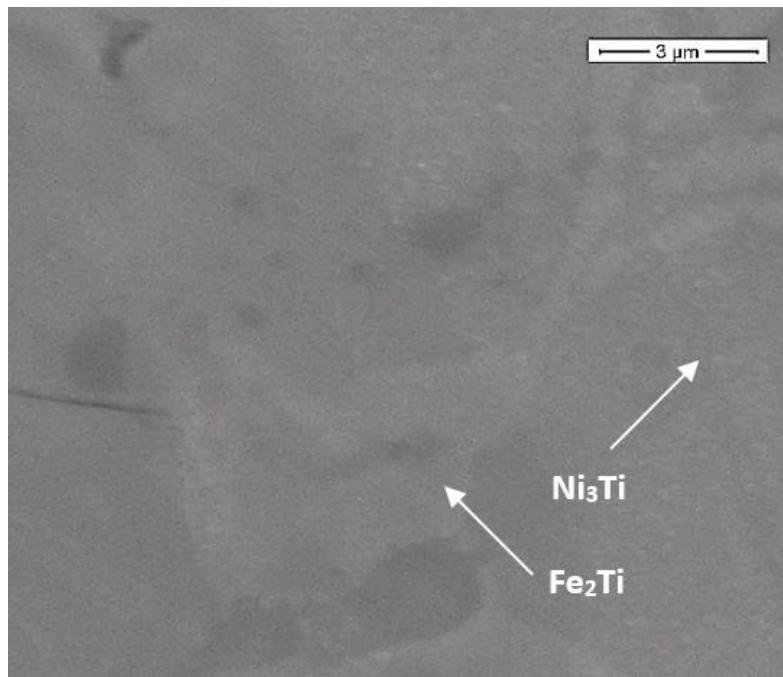


Fig. 4 SEM image of  $\text{Fe}_{35}\text{Ni}_{35}\text{Ti}_{30}$ . 20000x

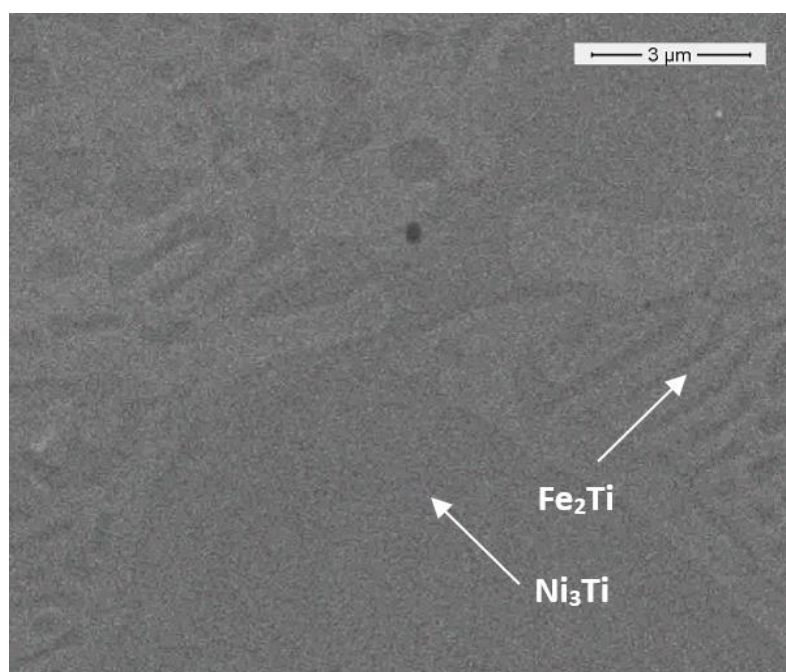


Fig. 5 SEM image of  $\text{Fe}_{30}\text{Ni}_{15}\text{Ti}_{30}\text{Cr}_5$ . 20000x

XRD phase analysis showed that in tested alloys there occur two phases -  $\text{Fe}_2\text{Ti}$  and  $\text{Ni}_3\text{Ti}$  (Fig. 5). In the case of the Cr doped alloy, the chromium dissolved in the matrix, without forming known compounds (Fig. 6).

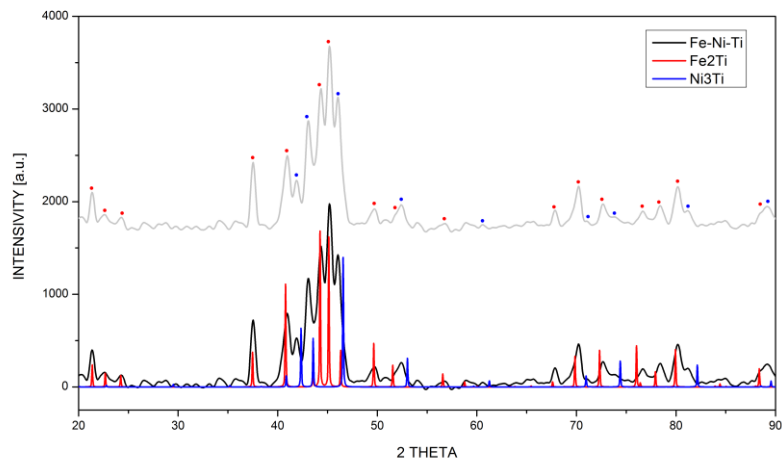


Fig. 6 X-ray diffraction patterns of  $Fe_{35}Ni_{135}Ti_{30}$

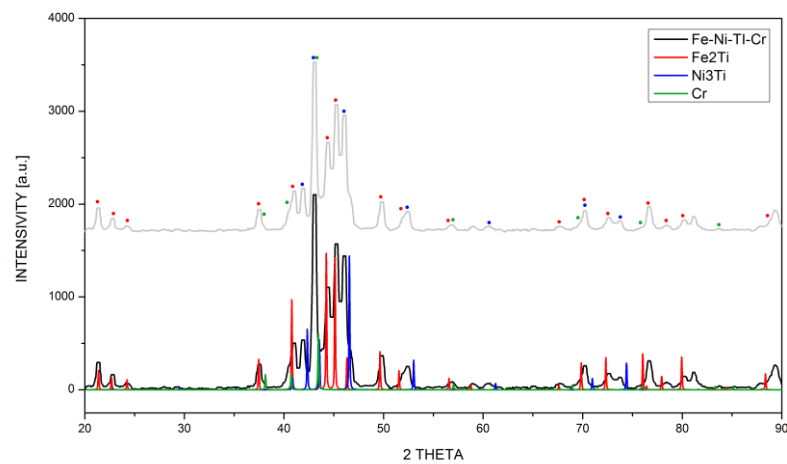


Fig. 7 X-ray diffraction patterns of  $Fe_{30}Ni_{135}Ti_{30}Cr_5$

The composition of  $Fe_{35}Ni_{135}Ti_{30}$  is on shared  $Fe_2Ti$  and  $Ni_3Ti$  phase region in the isothermal section diagram, as marked with red point. Fig 8 presents the DSC curve of heating-cooling process with sample mass 48.3 mg ( $Fe_{35}Ni_{135}Ti_{30}$ ) and 47.6 mg ( $Fe_{30}Ni_{135}Ti_{30}Cr_5$ ).

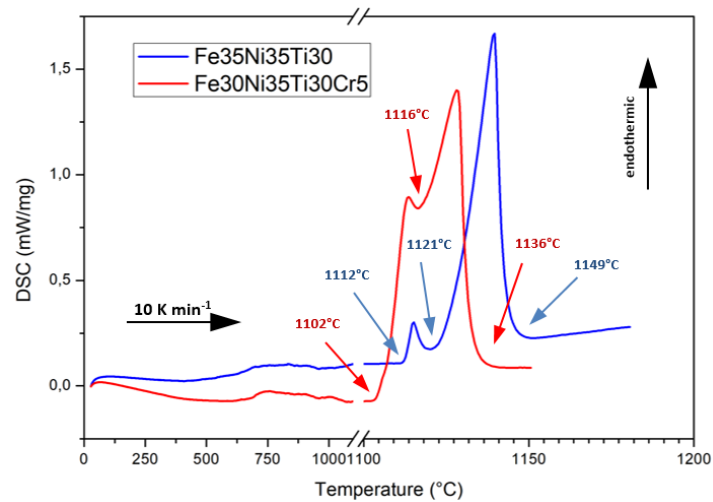


Fig. 8 DSC curve of  $Fe_{35}Ni_{135}Ti_{30}$  and  $Fe_{30}Ni_{135}Ti_{30}Cr_5$

During heating two endothermic peaks occur. Both corresponds to the same phenomena. The liquidus temperature is 1149°C ( $\text{Fe}_{35}\text{Ni}_{35}\text{Ti}_{30}$ ) and 1136°C ( $\text{Fe}_{30}\text{Ni}_{35}\text{Ti}_{30}\text{Cr}_5$ ). The lowest peak at 1112°C ( $\text{Fe}_{35}\text{Ni}_{35}\text{Ti}_{30}$ ) and 1102°C ( $\text{Fe}_{30}\text{Ni}_{35}\text{Ti}_{30}\text{Cr}_5$ ) alloy matches the ternary eutectic transition  $\text{Fe}_2\text{Ti} + \text{Ni}_3\text{Ti} \rightarrow \text{L}$  [8].

The mechanical properties of  $\text{Fe}_{35}\text{Ni}_{35}\text{Ti}_{30}$  and  $\text{Fe}_{30}\text{Ni}_{35}\text{Ti}_{30}\text{Cr}_5$  alloys were determined on the basis of nanoindentation tests. This type of experiment has an instrumental character, so during the described measurements the system continuously registers the load curve as a function of the current depth of the indenter. The load curves for  $\text{Fe}_{35}\text{Ni}_{35}\text{Ti}_{30}$  and  $\text{Fe}_{30}\text{Ni}_{35}\text{Ti}_{30}\text{Cr}_5$  alloys are shown in Fig. 9. The irregularities in course of the curve are caused by the multi-phase character of the material.

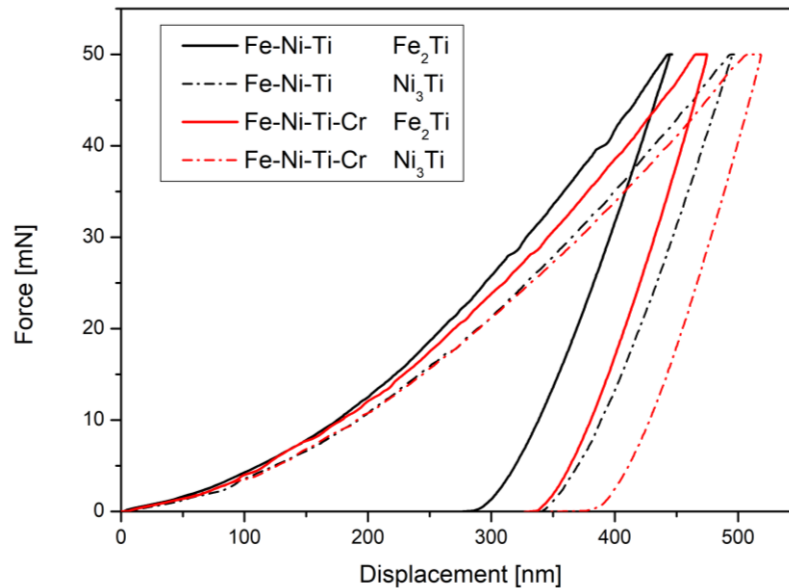


Fig. 9 Load – indenter depth function for Fe-Ni-Ti and Fe-Ni-Ti-Cr alloys.

The Berkovich tip impression is visible on optical image for  $\text{Fe}_2\text{Ti}$  phase (Fig. 10) and  $\text{Ni}_3\text{Ti}$  phase (Fig 11) for a single measurement. There is visible a difference between both impressions since both phases differ in hardness.

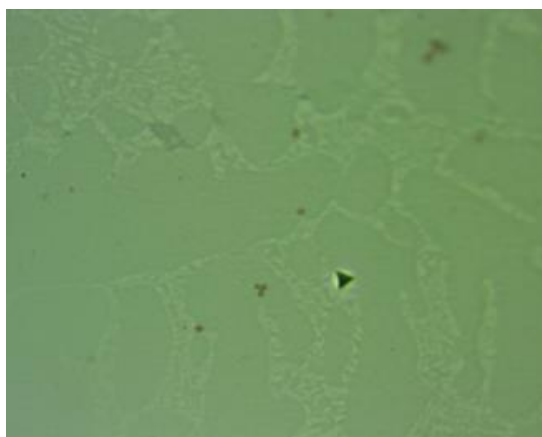


Fig. 10 LM image of the Berkovich tip impression –  $\text{Fe}_2\text{Ti}$  phase

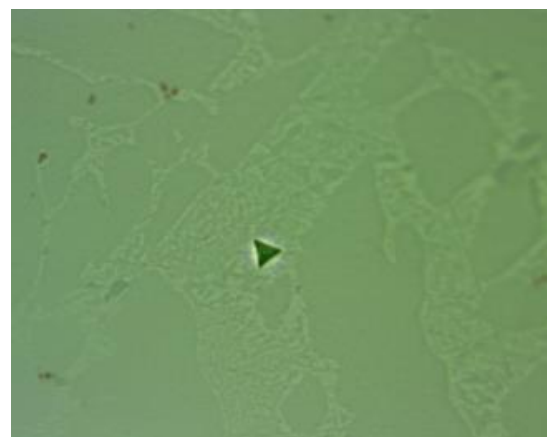


Fig. 11 LM image of the Berkovich tip impression –  $\text{Ni}_3\text{Ti}$  phase

The information is gained both about the plastic behavior of the tested material during loading and about its flexible behavior during unloading. Hardness of the material (resulting from the maximum depth of the indenter) as well as the Young's modulus (resulting from the character of the curve during unloading) was determined (Tab. 3).

Tab. 3 Summary of mechanical parameters estimated from nanoindentation tests for  $Fe_{35}Ni_{35}Ti_{30}$  and  $Fe_{30}Ni_{35}Ti_{30}Cr_5$  alloys ( $H_{IT}$  – instrumented hardness,  $HV_{IT}$  – instrumented Vickers hardness,  $E_{IT}$  – instrumented Young's modulus)

Alloy	Phase	$H_{IT}$ [MPa]	$HV_{IT}$ [HV]	$E_{IT}$ [GPa]
FeNiTi	$Fe_2Ti$	14983	1387	221
	$Ni_3Ti$	11561	1070	193
FeNiTiCr	$Fe_2Ti$	11972	1108	230
	$Ni_3Ti$	9768	904	212

Based on the obtained results, it can be concluded that the addition of chromium influenced the reduction of the instrumental hardness on the basis of tests of both alloys in the alloy -  $Fe_2Ti$  phase hardness decreases from 14983 [MPa] to 11972 [MPa] for chromium sample and  $Ni_3Ti$  phase from 11561 [MPa] to 9768 [MPa] for the sample without chromium. The decrease in hardness seems to be caused by the fragmentation of the microstructure generated by the presence of metallic chromium. In the case of Young's modulus, the reverse effect is noticeable - the addition of chromium influences the increase of this parameter for both alloys in the alloy - in the case of  $Fe_2Ti$  an increase of 9 GPa is noticeable, while for the  $Ni_3Ti$  phase an increase by almost 20 GPa was noted.

An interesting parameter possible to determine in the nanoindentation test is the share of plastic and elastic strain energy (Tab. 4). The Cr-containing sample, with lower hardness, is also characterized by less deformation energy than the chromium-free alloy. It is worth noticing that the ratio of elastic strain energy to total strain energy is different in both samples which indicates a different mechanical response of the tested samples to the penetration of the indenter.

Tab. 4 Summary of energy estimated from nanoindentation tests for  $Fe_{35}Ni_{35}Ti_{30}$  and  $Fe_{30}Ni_{35}Ti_{30}Cr_5$  alloys ( $W_{elast}$  – elastic strain energy,  $W_{plast}$  – plastic strain energy)

Alloy	Phase	$W_{elast}$ [pJ]	$W_{plast}$ [pJ]	$W_{elast}/W_{tot}$ [%]	$W_{plast}/W_{tot}$ [%]
FeNiTi	$Fe_2Ti$	3260	4997	39	61
	$Ni_3Ti$	3229	6004	35	65
FeNiTiCr	$Fe_2Ti$	2871	6236	32	68
	$Ni_3Ti$	2757	7427	27	73

The paper includes also the overall hardness measurements. They were performed with Vickers method, applied to 100 measure points distributed evenly. Resulting histograms are presented below (Fig. 12, Fig 13).

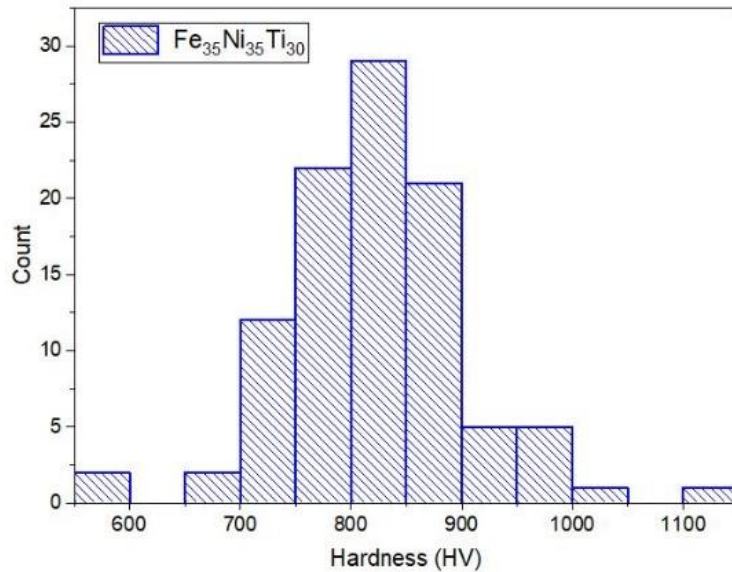


Fig. 12 Hardness histogram of  $Fe_{35}Ni_{35}Ti_{30}$

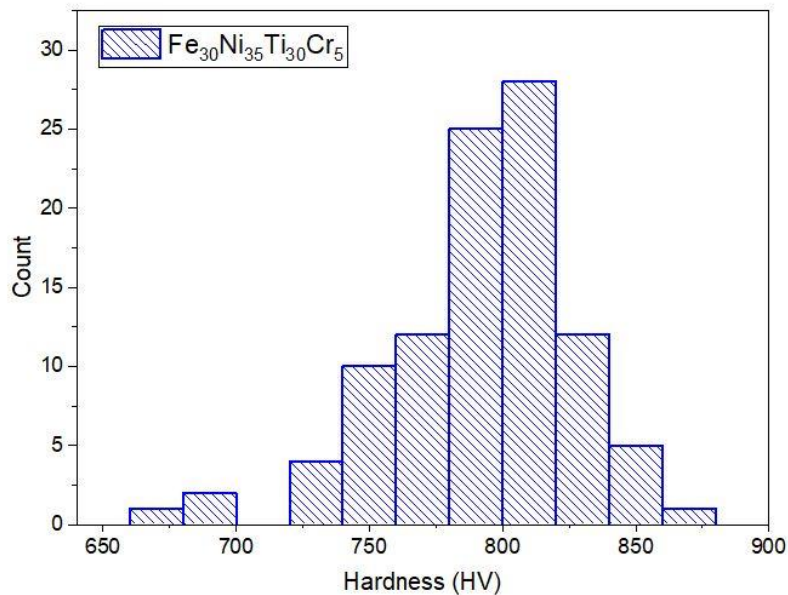


Fig. 13 Hardness histogram of  $Fe_{30}Ni_{35}Ti_{30}Cr_5$

Estimated hardness of  $Fe_{35}Ni_{35}Ti_{30}$  is 825 HV and for  $Fe_{30}Ni_{35}Ti_{30}Cr_5$  it is 812 HV. The obtained distribution of measurement results is similar to the Gaussian distribution with a distinctive dominant compartment. Based on the measurement results, a homogeneous hardness distribution for the manufactured alloys can be assumed. However, the lack of the symmetry is caused by multi-phase structure, not identified due to size of the tip impression. Because of that the measured hardness is the overall hardness of the material.

## 5. Conclusions

Laves phase was detected in both alloys:  $\text{Fe}_{35}\text{Ni}_{35}\text{Ti}_{30}$  and  $\text{Fe}_{30}\text{Ni}_{35}\text{Ti}_{30}\text{Cr}_5$ . For this reason, there exists a good correlation of the result shown in paper with the literature.

The data present diphasic structure which was proven by means of SEM and XRD techniques. SEM analysis detected varying distribution of elements on the surface. EDS distinguished Fe-Ti and Ni-Ti rich regions which further were associated with  $\text{Fe}_2\text{Ti}$  and  $\text{Ni}_3\text{Ti}$  phases by XRD diffractograms. Moreover, DSC also confirmed diphasic nature of both alloys.

The addition of chromium reduces the melting point in the Fe-Ni-Ti-Cr alloy. Cr is uniformly distributed over the surface which apparently diverse structural and mechanical properties of phases occurring in the compared materials.

In relation to the  $\text{Fe}_{35}\text{Ni}_{35}\text{Ti}_{30}$ , in the chromium doped alloy decrease in instrumental hardness was observed. Lower hardness causes lower deformation energy than in base alloy. On the other hand, Young's modulus increases about 10 GPa within  $\text{Fe}_2\text{Ti}$  phase and about 20 GPa within  $\text{Ni}_3\text{Ti}$ . All of that indicates different mechanical responses of the samples to the indenter penetration.

Both alloys were characterized by approximately the same hardness within the entire sample section. It means that the tip impression of the indenter was greater than the phase size and only the overall hardness was measured, then. The addition of chromium to the chemical composition causes a decrease in the hardness of the alloy.

## References

- [1] Cacciamani, G. and De Keyzer, J. and Ferro, R. and Klotz, U.E. and Lacaze, Jacques and Wollants, P. Critical evaluation of the Fe-Ni, Fe-Ti and Fe-Ni-Ti alloy systems. *Intermetallics*, vol. 14 (n° 10 - 11). pp. 1312-1325, 2016, ISSN 0966-9795.
- [2] Karhik G, Kashyap B, T Ram Prabhu Processing, properties and applications of Ni-Ti-Fe. *Materials Today: Proceedings*. 2017.
- [3] Mantovani D. Shape memory alloys, Properties and biomedical applications, *Journal of the Minerals, Metals and Materials Society*, 52, 36-44, 2000.
- [4] Zhong Zhou, Yajun Liu, Guang Sheng, Fuyue Lei, Zhitao Kang. A contribution to the Ni-based mobility database: Fcc Ni-Fe-ti ternary alloy. *CALPHAD: Computer Controlling of Phase Diagrams and Thermochemistry*, 2014.
- [5] Gaşior W, Dębski A. Enthalpy of formation of intermetallic phases from Fe-Ni-Ti system. Comparative studies. *Archives of metallurgy and materials*, volume 57, issue 4, 2012.
- [6] Gautam Ghosh, *Iron-Nickel-Titanium*. Landolt-Börnstein New Series IV/11A4.
- [7] Pelloth J, Brand R. A, Keune W. Local magnetic properties of the  $\text{Fe}_2\text{Ti}$  Laves phase. *Journal of Magnetism and Magnetic Materials* 140-144, 59-60, 1995.
- [8] Ying Ruan, Haizhe Zhu, Qingping Wang, Fuping Dai, Delu Geng, Bing Wei Dendrite growth and micromechanical properties of rapidly solidified tetrary Ni-Fe-Ti alloys *Natural Science: Materials International* 27, p 635-639, 2017
- [9] *ASM Handbook Volume 2: Properties and Selection: Nonferrous Alloys and Special-Purpose Materials*, ASM International, ASM International, 1990 p. 599-606 ISBN: 978-0-87170-378-1